Self-assembly of Gold Nanoparticles Using HPI S-layer Proteins Biotemplate

M. Abdolirad[a], R. Khalilzadeh[b],* and M. Alijanianzadeh[c]

[a]Faculty of Chemistry and Chemical Engineering, Malek-Ashtar University of Technology, Tehran, Iran
[b]Faculty of Chemistry and Chemical Engineering, Malek-Ashtar University of Technology, Tehran, Iran
[c]Department of Cell & Molecular Biology, Faculty of Biological Sciences, Kharazmi, Karaj, Iran

ABSTRACT

Bacterial cell-surface proteins (S-layer proteins) have an extremely repetitive surface structure well suited as a biotemplate to fabricate metallic/semiconducting nanostructures; an issue of high importance to the electronic industry. The surface layer proteins of *Deinococcus radiodurans R_1* (HPI) is an attractive S-layer for arraying nanoparticles. It illustrates hexagonal symmetry which is composed of a hexameric protein core unit with a middle hole. In this study, hexagonally structure of HPI protein was confirmed by AFM. Transmission electron microscopy and Fourier transform analysis revealed the formation of hexagonally ordered arrays of 4.5 nm citrate-capped Au nanoparticles. Also, the influence of stability and dispersity of gold nanoparticles has been investigated on the fabrication of ordered arrays by nanoparticle's zeta potential. The results reflect the effect of nanoparticles' zeta potential value on the creation of their ordered arrays through HPI layer, which could be useful in using these ordered nanoarrays for fabricating bio-sensors and some electronic devices.

INTRODUCTION

Fabricating structures and arrays in nanoscale for miniaturizing of electronic devices has been a major challenge in the recent decades. Several approaches composed of biological or non-biological methods have been used. Among non-biological methods, lithography techniques can create ordered arrays of nanoparticles/nanostructures in nonoscale and control the size and spacing of particles (≤ 100 nm features) but being expensive and low speed are the main reasons of their limited application. In addition to these methods, biological methods such as DNA [1,2], ferritin [3] and viruses [4,5] have been exploited to create ordered nanoarrays of gold nanoparticles, particles, quantum dots and nanowires.Although these methods can be beneficial to create ordered nanostructures but an alternative approach is using other kinds of proteins that can spontaneously self-assemble to form a two-dimensionalarray with large surface area.One example of self-assembled proteins are the Surface layers (S-layers).

S-layer proteins make the outer component of prokaryotes cell wall and are the most proteins produced by cells. They are consisted of periodical repetition of the same protein (or glycoprotein) subunits with a molecular weight of 40-200 kDa dependent on the particular microbial species. S-layer lattices display oblique, square or hexagonal symmetries and pores with similar size and morphology in the range of 2-8 nm. Surface layers topography and physicochemical properties are often diverse between the inner face attached to the cell, and outer face exposed to the external environment [6-12].

Based on the significant inherent feature of S-layers to self-assemble into 2-dimensional arrays in suspension and at interfaces [13,14], they are considered in interesting applications of biotechnology and nanobiotechnology [9,10, 15-17]. However many other proteins also assemble into 2-dimensional crystals [18], but unique surface topography, chemical properties and high repeated structure of S-layer proteins help them be suitable as a biotemplate to create nanostructures and metallic/semiconductor arrays. These arrays are crucial to the enhancement of electronic and optic devices' nonlinear optic properties.

*Corresponding author. E-mail: rkhalilzadeh@mut.ac.ir

An interesting S-layers template is HPI layer of *Deinococcus radiodurans* which was used in the past to fabricate ordered arrays of metallic and semiconductor nanoparticles such as Au, Pt, CdSe/ZnS [19-25]. The Hpi lattice displays hexagonal symmetry with a 2 nm central pore and a distance of 18nm among pores. The structure of Hpi has been analyzed by electron microscopy [26-28] and AFM [29-32]. AFM analyses demonstrate the hydrophobic inner face of the surface layer while the outer face is partly hydrophilic [29].

The biomolecules such as Hemoglobin [33,34] and human serum albumin [35,36] have been used as suitable model system to study their interaction with other small molecules and design drugs, because of their developed both structural and functional aspects.Unfortunately, the lack of any high-resolution 3-D structural data and very limited information about the physical/biochemical characteristics of the HPI S-layers make it difficult to determine which particular S-layer amino acids are exposed to solvent and are the likely candidates of interactions with nanoparticles

The creation of long-range ordered arrays of nanoparticles with a more highly uniform appearance,depends on different parameters including the relevant solution deposition conditions (affecting particle binding on the S-layers, *e.g.*, ionic strength, nanoparticles concentration), the nanoparticles synthesis conditions (to achieve a higher degree of particle monodispersity), improvement of site-specific binding of functionalized nanoparticles, *etc*. Some of these parameters were investigated by other researchers [37,38]. Previously, the interaction between lysozyme and silver nanoparticles has been studied by spectroscopic and zeta potential techniques [39]. In this paper,transmission electron microscopy (TEM) and Fourier transform analysis are used to study the effect of the zeta potential of gold nanoparticles on their arrays' formation which has not been investigated before.

MATERIALS AND METHODS

Cultivation of Microorganism

D. radiodurans R₁ was purchased from Iranian Biological and Genetic Resource National Center. It was cultured in the 1 l growth media (10 g Tryptone, 5 g glucose, 5 g yeast extract, 5 g NaCl) in incubator-shaker at 30 °C under agitation (180 rpm). Growth was traced by evaluating the optical density of the solution at 600 nm. Cells were harvested at early stationary phase by centrifugation at 7000 × g for 10 min, thenwere washed two times with resuspension in deionized water.

S-layer Protein Purification

HPI proteins were purified by performing differential centrifugation. Cells were stripped of their S-layers by incubation in 2 wt% lithium dodecyl sulfate (LDS) for 4 h at 4°C [38]. The suspension was centrifuged at 3000 g for 15 min to remove denuded cells, and the supernatant was conveyed to fresh centrifuge tubes. HPI proteins were sedimented by centrifugation at 20000 g for 30 min. To obtain HPI-layer sheets free of any associated proteins, pelleted proteins were incubated in 2% SDS at 60 °C for 30 min [40]. The HPI layers were sedimented by centrifugation at 20000 g for 30 min. The HPI sheets were washed several times in DI water by the same repeated resuspension-centrifugation. The HPI layer stock solution (~0.5 mg ml^{-1} protein in ultrapure de-ionized water) was kept at 4 °C until next use.

S-layer proteins concentration was estimated based on the Bradford assay applying bovine serum albumin (BSA) as the standard [41].

Atomic Force Microscopy

Atomic force microscope (ARA-AFM, Ara-Research, Iran) was utilized for topographic imaging of samples. Imaging was performed in tapping mode with NSC36/Al BS silicon tip (Mikro Masch Company).

Nanoparticles

4.5 nm citrate capped gold nanoparticles with zeta potential of -13 mV and -35 mV were procured from Taknam Company (registered trademark in Iran).

UV/visible Absorption Spectroscopy

Ultraviolet/visible spectra were acquired by UV-Vis spectrophotometer (Biochrom Ltd., Cambridge UK), with spectral resolution of 1 nm in the visible region.

Zeta potential Measurements

The zeta potential of gold nanoparticles was measured using Zetasizer Nano instruments (Malvern, UK) to determine the surface charge of them.

Gold Nanoparticles Patterning

Ordered gold (Au) nanoparticles were patterned hexagonally by exploiting the HPI surface layer as a biotemplate. In this procedure, 50 µl drops of 10 mM sodium citrate buffer solution (pH 8) containing HPI S-layer proteins at a concentration of 50 µg ml^{-1} were placed onto TEM grids for 1 h at room temperature and then rinsed softly with DI H$_2$O. Immediately after the rinsing steps, each grid (now coated with S-layer protein) was immersed in a solution of 4.5 nm citrate-stabilized gold nanoparticleswith different zeta potential (-13 mV and -35 mV). After 30 min, a short rinsing step in DI H$_2$O was done to remove loosely adsorbed nanoparticles. Ultimately, samples were dried and imaged by transmission electron microscopy.

Transmission Electron Microscopy

Transmission electron microscopy (TEM) was performed using an EM10C transmission electron microscope (Zeiss Company, Germany) operating at an accelerating voltage of 80 kV. For TEM imaging, carbon-coated Formvar grid substrates were used to adsorb native HPI layer fragments.

Image Processing and Fourier Transform Analyses

The analyses of all images were done by ImageJsoftware(https://imagej.nih.gov/ij/, NIH, University of Wisconsin). For biotemplating experiments, nanoparticle surface coverage measurements were accomplished first by determining a region on the S-layer and next doing a threshold/particle analysis of TEM images using ImageJ to measure the number of particles per square micrometer. Also,the symmetry of patterned Au nanoparticles through HPI layer was determined by analyzing 2-D fast Fourier transforms (FFT)of TEM images of the biotemplated nanoparticles in ImageJ. For FFT analyses, a region of interest for each nanoparticle array image was digitally selected before doing the FFT process.

RESULTS AND DISCUSSION

Characterization of Native S-layer Protein Lattices

Primary analyses to confirm the integrity and lattice dimensions of the purified HPI layer were performed using tapping mode AFM. AFM imaging of S-layer fragments on freshly cleaved mica revealed the expected hexagonal structure of HPI which is consisted of periodic repetition of the same protein (or glycoprotein) subunits (Fig. 1a). From analyses of AFM images, the lattice constant of HPI was determined 18.2 nm which confirmed homogeneity of HPI lattice (Fig. 1b). And also, FESEM analysis of HPI fragments confirmed the hexagonal structure of HPI sheets. Which were presented in our previous work [42] and consistent with other findings [30].

Characterization of Gold Nanoparticles

Based on literature findings gold nanoparticles with negative surface charge can be patterned by HPI sheets and create hexagonal arrays [38]. So in this study, gold nanoparticles withzeta potential of -13 mV and -35 mV have been used to investigate the influence of zeta potential value on arraying gold nanoparticles by HPI protein biotemplate.

Figure 2a and Fig. 3a show TEM images of uniform and 4.5 nm size of presynthesized gold nanoparticles with -13 mV and -35 mV zeta potential, respectively. UV-Vis absorption spectra of gold nanoparticles in Fig. 2b and Fig. 3b show the formation of gold nanoparticles. The negative surface charge of citrate-stabilized Au nanoparticles and its intensity can be confirmed with the zeta potential measurements (Figs. 2c and 3c).

Nanoparticle Patterning on HPI S-Layers

According to previous studies, two distinct adsorption patterns have been observed, namely random and ordered patterns of nanoparticles. Based on literature review, two different adsorption patterns are related to the binding of NPs to the two different faces of the S-layer protein sheets. It is displayed that nanoparticle films have been formed by electrostatic attractions. In these experiments, the periodically arranged functional groups which located on S-layer sheets are site-specific for anchoring nanoparticles [38].
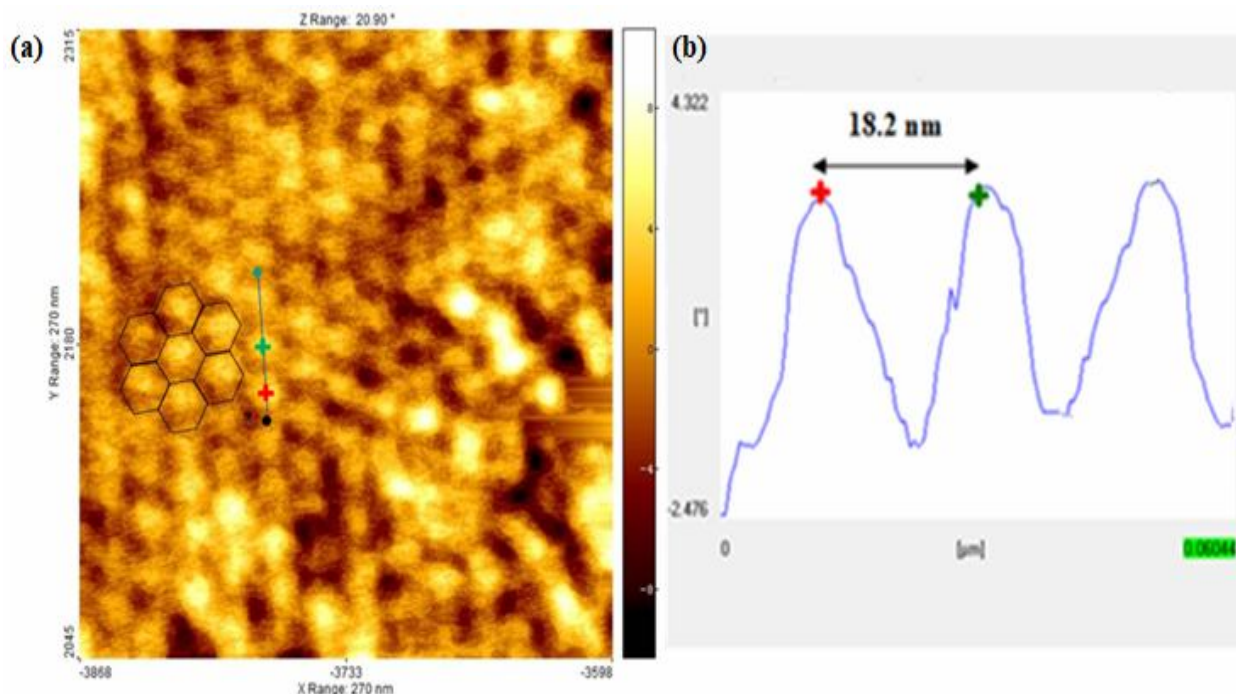
Fig. 1. (a) AFM image of HPI layer topography. Black lines show the hexagonally structure of HPI and red and green signs show the size of lattice constant. (b) Analysis profile of the area marked by the red and green signs in the image (a).

Our approach here was using Au nanoparticles with different zeta potentialsto survey their self-assembly onto HPI S-layer proteins pre-immobilized on TEM grid substrates. In all experiments,a significantly higher amount of particles' binding was found in the areas of the grid containing S-layers compared to the bare surface of the TEM grid background in TEM image analyses. The first set of nanoparticle biotemplating experiments were performed by Au nanoparticles with -13 mV zeta potential using the HPI surface layer. Figure 4 shows the TEM image of patterned Au nanoparticles with -13 mV zeta potential on HPI S-layer. The 2-D FFT spectrum (Fig. 4) of the ordered domains exhibits a hexameric symmetry pattern which confirms the presence of a dominant 6-fold symmetry. Black circulars in Fig. 4 show ring type structure formed by a group of nanoparticles. At several locations, some of the S-layer bound Au nanoparticles seem to be aggregated together forming small clusters comprised of 2-3 closely spaced particles (with < 2 nm interparticle edge-to-edge

distance (indicated by black arrows in Fig. 4)).

In the second experiment Au nanoparticles with -35 mV zeta potential were used to pattern by HPI S-layer. Figure 5 illustrates the TEM image of Au nanoparticles with -35 mV zeta potential which were patterned on HPI sheets. The 2-D FFT spectrum (Fig. 5) of the ordered domains demonstrates a hexameric symmetry pattern.

In this experiment, the strong peak reflections found in the corresponding FFT spectra (inset to Fig. 5) confirm that Au nanoparticles with -35 mV zeta potential have created a mostly 6-fold orientation symmetry. Furthermore, as it has been illustrated in Fig. 5 the number of spots in the FFT spectrum is higher than Fig. 4 which confirms the higher level of ordering of nanoparticles with -35 mV zeta potential on the HPI template.

As depicted in Fig. 4, low repulsion force of nanoparticles caused a high level of aggregation of the nanoparticles with -13 mV zeta potential and their tendency to each other on HPI layer compared to when the
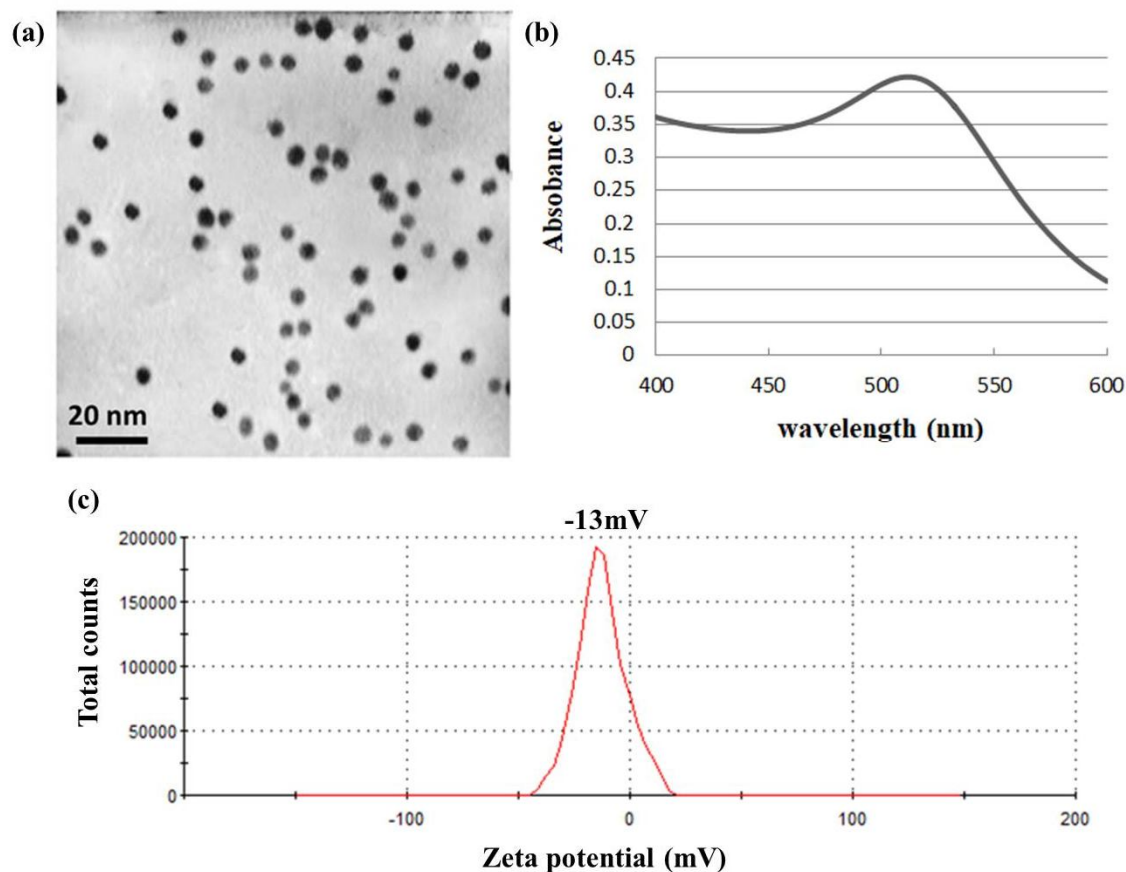
Fig. 2. (a) TEM image (b) UV-Vis absorption spectra (c) Zeta potential measurement of 4.5 nm citrate stabilized gold nanoparticles with -13 mV zeta potential.

experiments were performed by nanoparticles with -35 mV zeta potential.

In Fig. 4 there are nanoparticles which are absorbed nonspecifically to HPI template and this could be due to the low stability of nanoparticles with -13 mV zeta potential and poor interaction between nanoparticles and functional groups on HPI template.

Well dispersion of nanoparticles with -35 mV zeta potential and strong interaction between nanoparticles and functional groups on HPI template caused high level of ordering of them on HPI template.

The overall surface coverage of bound nanoparticles for nanoparticles with -13 mV zeta potential was estimated about 6750 particles per square micrometer which is significantly higher than nanoparticles with -35 mV zeta

potential (about 3111 particles per square micrometer). It should be mentioned that the solution of nanoparticles with -13 mV zeta potential was diluted and the concentration of nanoparticles with -13 mV zeta potential was half of nanoparticles with -35 mV zeta potential. In the same concentration, the number of nanoparticles with -13 mV zeta potential which bounds to HPI template was strongly increased and no order was observed.

The creation of long-range ordered arrays displaying a more highly uniform appearance may eventually be achievable through several possible routes. The binding of the individual particles on the HPI template likely arises from a high intrinsic affinity between the citrate groups of the Au nanoparticles and various polar/charged functional groups located on the surface of S-layer protein monolayer.

156
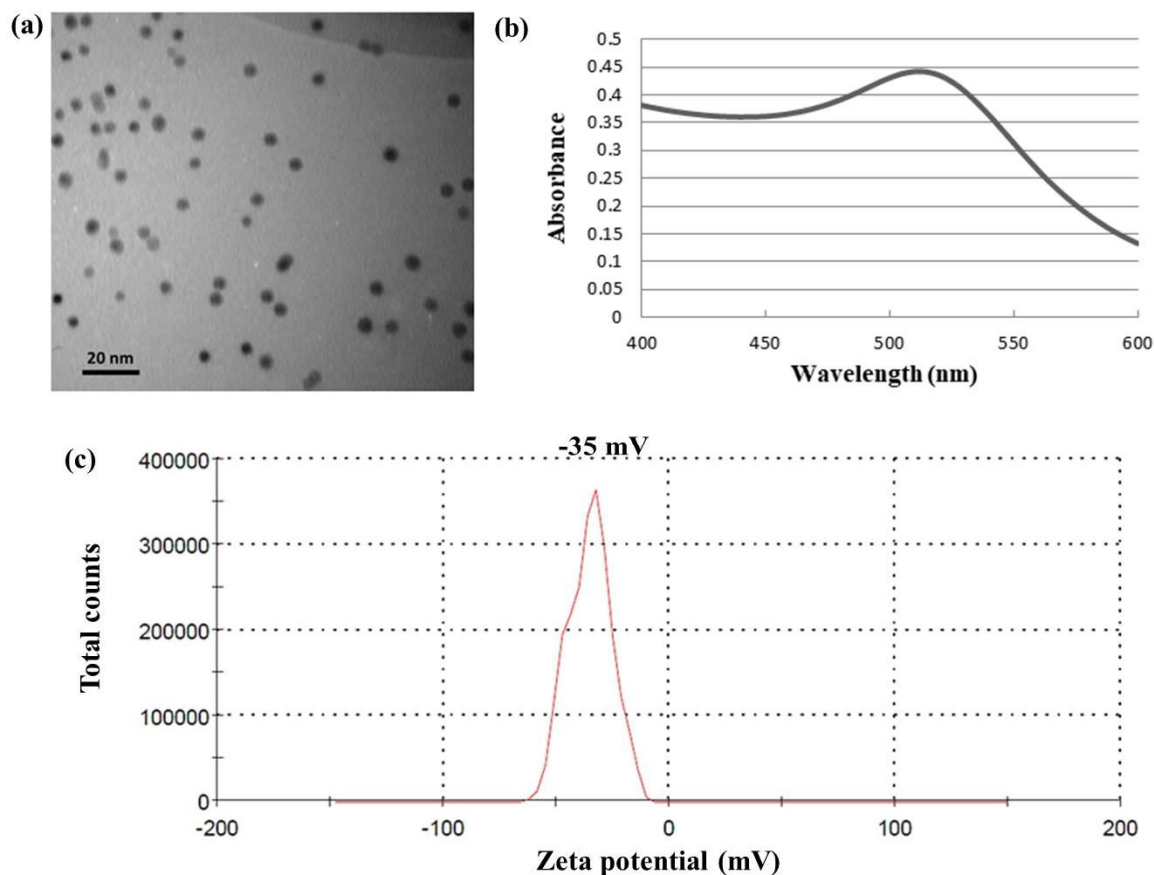
Fig. 3. (a) TEM image (b) UV-Vis absorption spectra (c) Zeta potential measurement of 4.5 nm citrate stabilized gold nanoparticles with -35 mV zeta potential.

The results showed that the level of dispersity of nanoparticle could affect their biotemplating onto HPI S-layer. This specifies that the electrostatic repulsive forces between like-charged nanoparticles with -13 mV zeta potential is not strong enough to keep the particles suspended, and therefore aggregation and precipitation occur. In addition, the intensity of interaction between nanoparticles and functional groups is low, so that the level of ordering of patterned Au nanoparticles with -35 mV zeta potential get higher than Au nanoparticles with -13 mV zeta potential.

The zeta potential is the stability level of particle charges. Zeta potential values of large magnitude are more stable than smaller values. The smaller values indicate that

particles will have a tendency to aggregate and the colloidal system is not stable because ofthe weak electrostatic repulsive force [43].

It should be mentioned that, the effect of the gold nanoparticles' zeta potential on their biotemplating by HPI layer has not been investigated previously. Eventually, the experimental results described in this article suggest that Au nanoparticles with high zeta potential seem to be the most optimal for the biotemplated synthesis of hexagonal ordered nanoparticle array structures using these S-layer proteins.
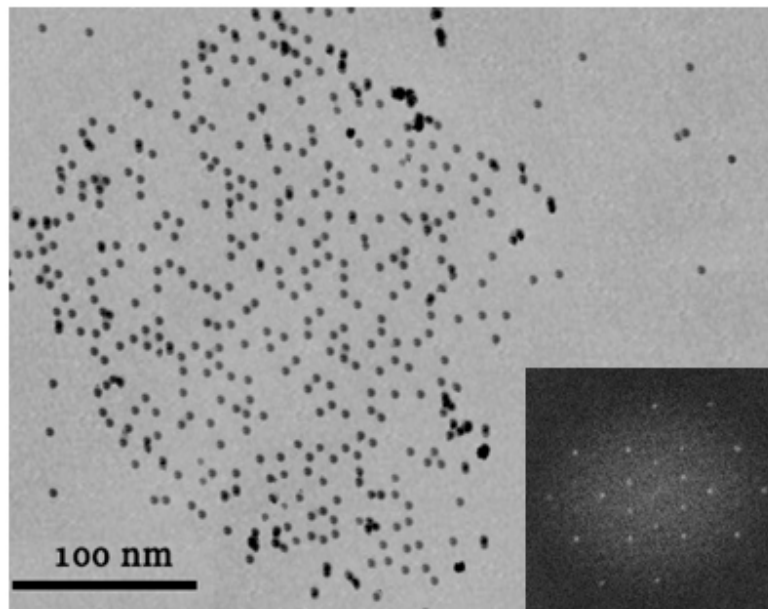
CONCLUSIONS

Hexagonal arrays of gold nanoparticles with low zeta
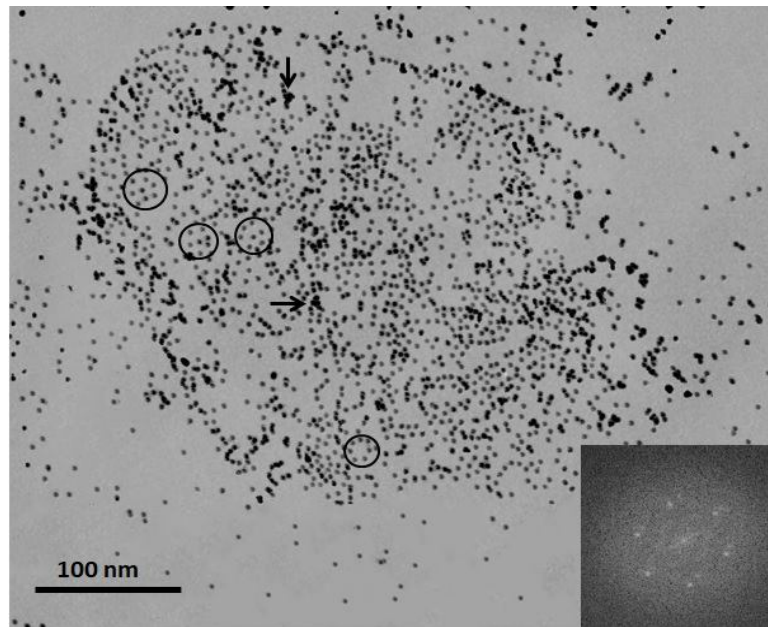
Fig. 4. TEM image of patterning Au nanoparticles with -13 mV zeta potential on HPI S-layer. TEM image contains FFT analysis which confirms the hexagonal order of gold nanoparticles. FFT spectra were calculated for a 350 nm-diameter circular region of the pattern. Black circulars show ring type structure formed by a group of nanoparticles. Black arrows show accumulation of nanoparticles.

Fig. 5. TEM image of patterning Au nanoparticles with -35 mV zeta potential on HPI S-layer. TEM image contains FFT analysis which confirms the hexagonal order of gold nanoparticles. FFT spectra were calculated for a 300 nm-diameter circular region of the pattern.

potential value on HPI layer displayed some aggregations and low level of ordering compared to hexagonal arrays of nanoparticles with high zeta potential value. Thus, the intensity of interaction between nanoparticles and protein's functional groupsand the stability of nanoparticles couldaffect their templating through HPI layer. The results of this study demonstrated a biotemplate-based approach for the fabrication of nanoarrays using gold nanoparticles. We anticipated that these ordered array structures can be useful in the development of miniaturized electronic devices.

ACKNOWLEDGEMENTS

Conflict of Interest

The authors declare that they have no conflict of interest.

REFERENCES

[1]   H. Nakao, H. Shiigi, Y. Yamamoto, S. Tokonami, T. Nagaoka, S. Sugiyama,T. Ohtani, Nano Lett. 3 (2003) 1391.

[2]   F. Patolsky, Y. Weizmann, O. Lioubashevski, I. Willner, Angew. Chem. 114 (2002) 2429.

[3]   Z. Yuan, D.N. Petsev, B.G. Prevo, O.D. Velev, P. Atanassov, Langmuir, 23 (2007) 5498.

[4]   S.-W. Lee, C. Mao, C.E. Flynn, A.M. Belcher 296 (2002) 892.

[5]   C. Mao, C.E. Flynn, A. Hayhurst, R. Sweeney, J. Qi, G. Georgiou, B. Iverson, A.M. Belcher, Proc. Natl. Acad. Sci. USA. 100 (2003) 6946.

[6]   U.B. Sleytr, B. Schuster, E.M. Egelseer, D. Pum, FEMS Microbiol. Rev. (2014) 1.

[7]   H. König, H. Claus, A. Varma (Eds.), Prokaryotic Cell Wall Compounds, Springer, Berlin, 2010.

[8]   M.C. Flickinger (Ed.), Encyclopedia of Industrial Biotechnology: Bioprocess, Bioseparation, and Cell Technology, John Wiley & Sons, Hoboken, 2009.

[9]   V. Debabov, Mol. Biol. 38 (2004) 482.

[10]   U.B. Sleytr, B. Schuster, D. Pum, IEEE Eng. Med. Biol. Mag. 22 (2003) 140.

[11]   M. Sara, U.B. Sleytr, J. Bacteriol. 182 (2000) 859.

[12]   G. Babolmorad, G. Emtiazi, R. Emamzadeh, Appl. Biochem. Biotechnol. 173 (2014) 103.

[13]   F. Baneyx, J.F. Matthaei, Curr. Opin. Biotechnol. 28 (2014) 39.

[14]   D. Pum, J. Toca-Herrera, U.B. Sleytr, Int. J. Mol. Sci. 14 (2013) 248.

[15]   N. Ilk, E.M. Egelseer, U.B. Sleytr, Curr. Opin. Biotechnol. 22 (2011) 824.16.

[16]   D. Pum, U. Sleytr, Trends Biotechnol. 17 (1999) 8.

[17]   U. Sleytr, M. Sara, P. Messner, D. Pum, Annl. NY. Acad. Sci. 745 (1994) 261.

[18]   B.K. Jap, M. Zulauf, T. Scheybani, A. Hefti, W. Baumeister, U. Aebi, A. Engel, Ultramicroscopy 46 (1992) 45.

[19]   Y. Sierra-Sastre, S.A. Dayeh, S.T. Picraux, C.A. Batt, ACS NANO 4 (2010) 1209.

[20]   Y. Sierra-Sastre, S. Choi, S.T. Picraux, C.A. Batt, J. Ame. Chem. Soc. 130 (2008) 10488.

[21]   S.S. Marka, M. Bergkvist, P. Bhatnagar, C. Welch, A.L. Goodyear, X. Yang, E.R. Angert, C.A. Batt, Colloids and Surf. B. 57 (2007) 161.

[22]   S.S. Mark, M. Bergkvist, X. Yang, L.M. Teixeira, P. Bhatnagar, E.R. Angert, C.A. Batt, Langmuir 22 (2006) 3763.

[23]   D.B. Allred, M. Sarikaya, F. Baneyx, D.T. Schwartz, Nano Lett. 5 (2005) 609.

[24]   E. Gyorvary, A. Schroedter, D. Talapin, H. Weller, D. Pum, U. Sleytr, J. Nanosci. Nanotechnol. 4 (2004) 115.

[25]   D.B. Allred, M. Sarikaya, F. Baneyx, D.T. Schwartz, Electrochim. Acta 53 (2007) 193.

[26]   W. Baumeistert, M. Barth, R. Hegerl, R. Guckenberger, M. Hahn, W. Saxton, J. Mol. Biol. 187 (1986) 241.

[27]   W. Baumeister, O. Koblert, Proc. Natl. Acad. Sci. USA 75 (1978) 5525.

[28]   E. Work, H. Griffiths, J. Bacteriol. 95 (1968) 641.

[29]   D.J. Muller, W. Baumeister, A. Engel, Proc. Natl. Acad. Sci. 96 (1999) 13170.

[30]   D.J. Muller, W. Baumeister, A. Enge, J. Bacteriol. 178 (1996) 3025.

[31]   S. Karrasch, R. Hegerl, J.H. Hoh, W. Baumeister, A. Engel, Proc. Natl. Acad. Sci. USA 91 (1994) 836.

[32] T.E. Lister, P.J. Pinhero, Langmuir 17 (2001) 2624.

[33] H. Sanei, A. Asoodeh, S. Hamedakbari-Tusi, J. Chamani, J. Solution Chem. 40 (2011) 1905.

[34] P. Mokaberi, V. Reyhani, Z. Amiri-Tehranizadeh, M.R. Saberi, S. Beigoli, F. Samandar, J. Chamani, New J. Chem. 43 (2019) 8132.

[35] Z. Sharif-Barfeh, S. Beigoli, S. Marouzi, A.S. Rad, A. Asoodeh, J. Chamani, J. Solution Chem. 46 (2017) 488.

[36] M. Zolfagharzadeh, M. Pirouzi, A. Asoodeh, M.R. Saberi, J. Chamani, J. Biomol. Struct. Dyn. 32 (2014) 1936.

[37] S.S. Mark, M. Bergkvist, X. Yang, E.R. Angert, C.A. Batt, Biomacromolecules 6 (2006) 1884.

[38] M. Bergkvist, S.S. Mark, X. Yang, E.R. Angert, C.A. Batt, J. Phys. Chem. B. 108 (2004) 8241.

[39] M. Kamshad, M. Jahanshah Talab, S. Beigoli, A. Sharifirad, J. Chamani, J. Biomol. Struct. Dyn. 37 (2019) 2030.

[40] R. Rachel, A. Engel, W. Baumeister, FEMS Microbiol. Lett. 17 (1983) 115.

[41] J.M. Walker, ed. The Protein Protocols Handbook. Springer Protocols Handbooks, Humana Press: New Jersey, 2002.

[42] M. Abdolirad, R. Khalilzadeh, M. Alijanianzadeh, Biomacromolecular J. 2 (2016) 126.

[43] M.R. Ivanov, H.R. Bednar, A.J. Haes, ACS NANO 3 (2009).